Constrained exact boundary controllability of a semilinear model for pipeline gas flow

Martin Gugat[1], Jens Habermann[2], Michael Hintermüller[3,4], Olivier Huber[4]

submitted: December 3, 2021

[1] Applied Analysis (Alexander von Humboldt–Professur)
    Friedrich–Alexander–Universität Erlangen–Nürnberg (FAU)
    Cauerstr. 11
    91058 Erlangen
    Germany
    E-Mail: gugat@fau.de

[2] Lehrstuhl für Mathematik
    Friedrich–Alexander–Universität Erlangen–Nürnberg (FAU)
    Cauerstr. 11
    91058 Erlangen
    Germany
    E-Mail: jens.habermann@fau.de

[3] Weierstrass Institute
    Mohrenstr. 39
    10117 Berlin
    Germany
    E-Mail: michael.hintermueller@wias-berlin.de

[4] Institut für Mathematik
    Humboldt–Universität zu Berlin
    Unter den Linden 6
    10099 Berlin
    Germany
    E-Mail: hint@math.hu-berlin.de
           olivier.huber@hu-berlin.de

Constrained exact boundary controllability of a semilinear model for pipeline gas flow

Martin Gugat, Jens Habermann, Michael Hintermüller, Olivier Huber

Abstract

While the quasilinear isothermal Euler equations are an excellent model for gas pipeline flow, the operation of the pipeline flow with high pressure and small Mach numbers allows us to obtain approximate solutions by a simpler semilinear model. We provide a derivation of the semilinear model that shows that the semilinear model is valid for sufficiently low Mach numbers and sufficiently high pressures. We prove an existence result for continuous solutions of the semilinear model that takes into account lower and upper bounds for the pressure and an upper bound for the magnitude of the Mach number of the gas flow. These state constraints are important both in the operation of gas pipelines and to guarantee that the solution remains in the set where the model is physically valid. We show the constrained exact boundary controllability of the system with the same pressure and Mach number constraints.

Introduction

Transition to renewable energy In the energy sector, policymakers in many countries have started to prepare a shift away from the use of nuclear or mostly fossil supplies to a portfolio with a strong emphasis on renewable energy resources. It is commonly agreed that for the pertinent transition period the optimized use of natural gas will be of paramount importance. This is substantiated by the currently known available gas resources as well as technical aspects such as transportability or storage capacity. Moreover, controlled market liberalization lies at the basis of an efficient distribution, with the latter clearly also benefiting from the currently available and planned system of pipelines. As a consequence a sound understanding of the transportation physics along with ways of (optimally) influencing the gas transport in pipelines is one of the main building blocks towards the optimal use of gas.

Mathematically, the flow of gas through pipes is modelled by the compressible Euler equations. As typically the diameter of a pipe is much smaller than the pipe's length one resorts to the study of a one-dimensional model, only. Moreover, the usual operating conditions of the pipeline network lead to an isothermal setting; see [1]. The resulting isothermal Euler equations form a quasilinear system of hyperbolic partial differential equations. Typically, in the operation of gas pipelines, the gas velocity is rather small while the gas pressure is high. Under such conditions, often a simpler semilinear model suffices. Correspondingly, based on an acoustic approximation of the isothermal Euler equations in this paper we derive a semilinear model which generates reasonable approximations of the state for sufficiently small Mach numbers and sufficiently high gas pressures without abrupt changes. Relying on assumptions on the problem data (physical characteristics of the pipe, initial and terminal states) the existence of solutions for this model is shown.

Given this existence result, the main result of this paper is concerned with constrained exact boundary controllability. In fact, we present assumptions that allow to control the gas flow from a continuous initial state to a continuous terminal state by suitably chosen boundary controls in such a way that during the whole process, bounds for the gas velocity and the gas pressure are satisfied. Such bounds are a standard requirement in the operation of gas pipelines. In our context, they have the additional effect that they guarantee that the states remain within the range where the semilinear model is valid. We illustrate the exact controllability result by numerical examples where the boundary controls for exact controllability are approximated with a numerical method of characteristics.

This paper has the following structure. In Section 1 we present the isothermal Euler equations. In Section 2 we derive the semilinear model, in Section 3 we consider the stationary solutions of the semilinear model. In Section 4 we first state the semilinear model in diagonal form. Then, we present our existence result for continuous solutions of the semilinear model that is based upon the characteristic curves. For certain system parameters we obtain continuous solutions for arbitrary long time intervals. In Section 5, we present our result on the exact controllability for the semilinear model. In Section 6, two numerical examples illustrate how the gas flow in a pipe can be transitioned between two stationary states using the approach introduced in the previous Section 5. Finally, conclusions are presented in Section 7.

1 The isothermal Euler equations

Consider a pipe of length $L > 0$ that corresponds to the interval $[0, L]$. Let $D > 0$ denote the constant diameter of the pipe, $\lambda_{fric} \geq 0$ the friction coefficient and $\varphi \in (-\infty, \infty)$ the slope. Define $s_{lope} := \sin(\varphi)$ and set $\theta := \frac{\lambda_{fric}}{D}$. Let g denote the gravitational constant, $\rho > 0$ the gas density, $p > 0$ the pressure and q the mass flow rate in $\text{kg s}^{-1}\,\text{m}^{-2}$. We assume that we have an ideal gas that satisfies the state equation

$$p = R_s^e\, T^e\, \rho,$$

where R_s^e is the gas constant and T^e is the temperature. The focus of our study is on the isothermal Euler equations (see for example [5])

$$\begin{cases} \rho_t + q_x = 0, \\ q_t + \left(p + \frac{q^2}{\rho}\right)_x = -\frac{1}{2}\theta\frac{q\,|q|}{\rho} - \rho\, g\, s_{lope}, \end{cases} \tag{1}$$

that govern the flow through a single pipe. In our analysis we also make use of the velocity $v = \frac{q}{\rho}$ and the sound speed c given by

$$\left(\frac{1}{c}\right)^2 = \frac{\partial\rho}{\partial p} = \frac{1}{R_s^e\, T^e}.$$

Thus, we have

$$c = \sqrt{R_s^e\, T^e}.$$

In what follows we concentrate on an ideal gas where the sound speed is constant. For the Mach number M this yields

$$M = \frac{v}{c} = c\,\frac{q}{p}.$$

Considering a *subsonic* flow regime, the absolute value of the velocity of the gas is strictly less than the sound speed in the gas. For the Mach number we thus have

$$|M| < 1.$$

This setting reflects the case that is relevant for gas transportation networks where upper bounds for the velocity of the gas are enforced in the operation of gas pipelines. In order to state (1) in terms of the dimensionless Mach-number M and the pressure p, we observe that

$$\rho = \frac{1}{c^2}\, p, \qquad q = \frac{1}{c}\, M\, p.$$

Hence, if $M \neq 0$, then the first equation of (1) yields

$$\ln(p)_t + (c\, M)\ln(|M|\, p)_x = 0. \tag{2}$$

Moreover, from the second equation of (1) we infer

$$\ln(p\,|M|)_t + \frac{c}{M}\left(1 - M^2\right)\ln(p)_x + 2\,c\,M\ln(p\,|M|)_x = -\frac{1}{2}\theta\,c\,|M| - g\,s_{lope}\,\frac{1}{c}\,\frac{1}{M}.$$

Note that multiplication by M yields an equation that is also well-defined for $M = 0$, namely

$$\frac{1}{p}(p\,M)_t + c\left(1 - M^2\right)\frac{p_x}{p} + 2\,c\,\frac{M}{p}(p\,M)_x = -\frac{1}{2}\theta\,c\,M\,|M| - g\,s_{lope}\,\frac{1}{c}.$$

2 The semilinear model for slow subsonic flow

Note that since $\ln(p)_t = \frac{p_t}{p}$, if the pressure p is sufficiently high and p_t is bounded, $\ln(p)_t$ is small. Equation (2) implies that if $\ln(p)_t$ is small (for example, close to a stationary state), $(c\,M)\ln(|M|\,p)_x$ is small. For Mach numbers with small absolute value, $\left(1 - (M)^2\right)$ is close to 1. Hence, if the pressure p is sufficiently large, p_t is bounded and for Mach numbers with small absolute value we can approximate the solution of the second equation of (1) by the solution of the equation

$$\ln(p\,|M|)_t + \frac{c}{M}\ln(p)_x = -\frac{1}{2}\theta\,c\,|M| - g\,s_{lope}\,\frac{1}{c}\,\frac{1}{M}. \tag{3}$$

For a solution of (1), due to (2), the error E on the left-hand side of (3) is

$$E = c\,M\ln(p)_x + 2\ln(p)_t.$$

This error is small if the time derivative p_t and the Mach number are sufficiently small, the pressure is sufficiently large, and p_x remains uniformly bounded. In [3], for the initial data $q(0,\,x) = 0$, $\rho(0,\,x) = \exp(\beta\,x)$ the solution of both the quasilinear and the semilinear models are given, which allows us to observe how the difference between the two solutions can grow exponentially fast with time.

For $M \neq 0$, define the matrix

$$A(M) = c\begin{pmatrix} 0 & M \\ \frac{1}{M} & 0 \end{pmatrix}.$$

In matrix notation, from (2) and (3) we obtain the model

$$\begin{pmatrix} \ln(p) \\ \ln(|M|\,p) \end{pmatrix}_t + A(M)\begin{pmatrix} \ln(p) \\ \ln(|M|\,p) \end{pmatrix}_x = \begin{pmatrix} 0 \\ -\frac{\theta}{2}\,c\,|M| - \frac{g\,s_{lope}}{c\,M} \end{pmatrix}. \tag{4}$$

Note that the eigenvalues of the system matrix $A(M)$ are $-c$ and c. In particular, they are constant.

Remark 2.1. *The eigenvalues of the quasilinear system* (1) *are $v + c$ and $v - c$. This implies that the error in the eigenvalues can only be small as long as $|v|$ (the absolute value of the Mach number M respectively) is sufficiently small.*

Since the first equation in (1) has not been modified, also (4) guarantees the conservation of mass. In terms of the physical variables p and q, the model (4) can be stated as the well–known semilinear model (see for example [6], [4]):

$$\begin{cases} \frac{1}{c^2}\,p_t + q_x = 0, \\ q_t + p_x = -\frac{1}{2}\theta\,c^2\,\frac{q\,|q|}{p} - g\,s_{lope}\,\frac{p}{c^2}. \end{cases} \tag{5}$$

Note that (5) is semilinear since the system matrix is constant whereas (4) is stated in quasilinear form.

3 The stationary states

In this section, we consider the stationary states of system (4). The stationary solutions of the quasilinear system (1) have been studied in [2]. For the stationary states of (4), there exists a constant C_s^e such that

$$|M|\, p = C_s^e.$$

Moreover, we have

$$
\begin{aligned}
\ln(p)_x &= -\frac{1}{2}\theta\, M\, |M| - g\, s_{lope}\, \frac{1}{(c)^2} \\
&= -\frac{1}{2}\theta\, (C_s^e)^2 \frac{1}{(p)^2}\mathrm{sign}(M) - g\, s_{lope}\, \frac{1}{(c)^2}.
\end{aligned}
$$

This yields

$$p_x = -\frac{1}{2}\theta\, (C_s^e)^2\frac{1}{p}\mathrm{sign}(M) - g\, s_{lope}\, \frac{1}{(c)^2}p.$$

For a horizontal pipe (that is $s_{lope} = 0$), we get

$$\left(\frac{p^2}{2}\right)_x = p\, p_x = -\frac{1}{2}\,\mathrm{sign}(M)\,\theta\,(C_s^e)^2.$$

Thus, for $x \in [0,\, L]$ we obtain

$$\frac{p^2}{2}(x) - \frac{p^2}{2}(0) = -\frac{1}{2}\,\mathrm{sign}(M)\,\theta\,(C_s^e)^2\, x.$$

This is the well-known WEYMOUTH equation. Note that for $M > 0$ the equation is a valid model only if x and consequently $L > 0$ are sufficiently small. Also, in the original model (1) for the stationary states a blow up of the derivative occurs after a finite length; see [2].

Now we consider the case where $s_{lope} \neq 0$. For a stationary state we still have $M\, p = C_s^e$. We obtain a *constant* stationary state if M is such that

$$M\, |M| = -\frac{2}{\theta\, c}\, g\, s_{lope}\, \frac{1}{c}.$$

This yields

$$M = -\mathrm{sign}(s_{lope})\,\sqrt{\frac{2}{\theta\, c}\, g\, |s_{lope}|\, \frac{1}{c}} =:\, \hat{M}.$$

In terms of physical variables, the constant stationary solution corresponds to a constant flow rate $\bar{q}$ and a constant pressure $\bar{p} > 0$ with

$$\bar{p}^2 = \frac{c^4\,\theta(\bar{q})^2}{2\, g\, |s_{lope}|}.$$

More generally, there exist stationary solutions with a constant flow rate $\bar{q}$ that satisfies

$$\mathrm{sign}(\bar{q}) = -\mathrm{sign}(s_{lope}) \tag{6}$$

where the pressure is given by

$$p(x) = \bar{p}\,\sqrt{1 + \hat{C}\,\exp\left(-2\, g\,\frac{s_{lope}}{c^2}\, x\right)},$$

as long as the term under the square root is positive with $\hat{C}$ chosen such that $p(0) > 0$ has the appropriate value. This can be verified by inserting the solution $(\bar{q}, p(x))$ into (5). More precisely, the definition of p implies

$$\frac{(p(x))^2 - \bar{p}^2}{\bar{p}^2} = \hat{C}\,\exp\left(-2\, g\,\frac{s_{lope}}{c^2}\, x\right).$$

Hence, due to the definition of $\bar{p}$, we have

$$
\begin{aligned}
p'(x) &= \frac{\bar{p}^2}{2} \frac{1}{p(x)} \hat{C} \exp\left(-2\,g\,\frac{s_{lope}}{c^2}\,x\right) \left(-2\,g\,\frac{s_{lope}}{c^2}\right) \\
&= \frac{\bar{p}^2}{2} \frac{1}{p(x)} \left(\frac{(p(x))^2}{\bar{p}^2} - 1\right) \left(-2\,g\,\frac{s_{lope}}{c^2}\right) \\
&= 2\,g\,\frac{s_{lope}}{c^2} \frac{\bar{p}^2}{2} \frac{1}{p(x)} - \frac{1}{2}\,2\,g\,\frac{s_{lope}}{c^2}\,p(x) \\
&= \text{sign}(s_{lope}) \frac{1}{2}\theta\,c^2\,\frac{\bar{q}^2}{p(x)} - g\,s_{lope}\,\frac{p(x)}{c^2}.
\end{aligned}
$$

Whence, the relation (6) implies that the second equation in (5) holds.

4   The semilinear model in diagonal form

In this section we state (4) in terms of the corresponding RIEMANN invariants. For the eigenvalues $\pm c$ of the matrix A we have the left-hand side eigenvectors

$$
l_\pm = (\pm p,\, M\,p).
$$

Multiplication of (4) from the left-hand side with $l_\pm$ yields

$$
(\pm p,\, M\,p) \begin{pmatrix} \ln(p) \\ \ln(|M|\,p) \end{pmatrix}_t \pm c\,(\pm p,\, M\,p) \begin{pmatrix} \ln(p) \\ \ln(|M|\,p) \end{pmatrix}_x
$$

$$
= -\frac{1}{2}\theta\,c\,M\,|M|\,p - g\,s_{lope}\,\frac{1}{c}\,p.
$$

We obtain the RIEMANN invariants

$$
R_\pm = \pm p + M\,p = (\pm 1 + M)\,p.
$$

Hence, the physical variables can be expressed in terms of the RIEMANN invariants as

$$
p = \frac{R_+ - R_-}{2}, \quad M = \frac{R_+ + R_-}{R_+ - R_-},
$$

and we have the flow rate

$$
q = \frac{1}{c}M\,p = \frac{1}{2\,c}(R_+ + R_-).
$$

Let us further define some notation. In fact, let $\sigma(z) := z\,|z|$ and consider the function

$$
F(x,\,y) := (x + y)\left|\frac{x+y}{x-y}\right| = (x - y)\,\sigma\left(\frac{x+y}{x-y}\right). \tag{7}
$$

Then, in terms of the RIEMANN invariants, the system has the diagonal form

$$
(R_\pm)_t \pm c(R_\pm)_x = -\frac{1}{4}\theta\,c\,F(R_+,\,R_-) - g\,s_{lope}\,\frac{1}{c}\,\frac{R_+ - R_-}{2}, \tag{8}
$$

which is well-defined as long as $R_+ \neq R_-$. In terms of the physical variables, this is equivalent to $p > 0$. This requirement is often satisfied, as in applications lower bounds $\underline{p} > 0$ for the pressure are often prescribed. In the subsonic flow regime, pressure constraints of the form

$$
\underline{p} \leq p \leq \bar{p} \tag{9}
$$

can be expressed in terms of the RIEMANN invariant as

$$2\underline{p} \leq R_+ - R_- \leq 2\bar{p}, \tag{10}$$

Similarly, whenever $2p = R_+ - R_- > 0$, the Mach number constraint

$$|M| \leq \lambda, \quad 0 < \lambda < 1, \tag{11}$$

is equivalent to

$$(1 + \lambda)R_+ + (1 - \lambda)R_- \geq 0, \tag{12}$$
$$(1 - \lambda)R_+ + (1 + \lambda)R_- \leq 0. \tag{13}$$

Moreover, with $p > 0$, it is easy to see that $|M| < 1$ implies that $R_+ > 0$ and $R_- < 0$. Note that all the constraints for the RIEMANN invariants are linear. This is convenient for associated optimal control problems for gas networks.

4.1 Existence of solutions of the semilinear model

The characteristic curves for the semilinear model are a priori given straight lines. Hence, the hyperbolic system is equivalent to a coupled family of integral equations along these characteristic curves. This allows to prove the existence of continuous solutions for continuous problem data using a fixed-point iteration with integration along the characteristic curves. The existence of broad solutions of the semilinear system has already been shown in [7] for the case of horizontal pipes. In [7], Proposition 4, lower and upper bounds for the pressures and for the flow rate are considered. Indirectly, this also yields bounds for the gas velocity and the Mach number. In this paper, in contrast to [7], we include sloped pipes in our analysis. Since the semilinear model is only valid for sufficiently small Mach numbers, we also include constraints for the Mach number directly in the analysis. We point out that such a constraint for the velocity of the gas is also used in practice to avoid vibrations of the pipelines. Note that in our result, all the constants in the assumptions are given explicitly, so they can be verified rather easily. Our result provides conditions that allow to obtain continuous solutions that satisfy the box constraints for the pressure and the Mach number. The conditions require continuous initial and boundary data that satisfy certain inequalities. Note that it is not sufficient to require that the initial and boundary data satisfy the state constraints for the pressure and the Mach number. This can be seen as follows: for a stationary state in a horizontal pipe, the pressure is decreasing along the pipe in the direction of flow. Hence, the pressure at the inflow end must be strictly above the lower bound for the pressure in order to guarantee that the state constraint is satisfied throughout the pipe.

In the forthcoming analysis, the inequality

$$\frac{\theta\lambda\sqrt{5}}{2} + \frac{g|s_{\text{lope}}|}{c^2} \leq \frac{1}{L} \tag{14}$$

between the physical characteristics of the pipe is the key to the existence of a solution. This explicit condition departs from the previous conditions for existence of solution, albeit with higher regularity.

Remark 4.1. *This condition is easy to check for existing networks. For instance, we can use the GasLib[1] dataset [12]. We focus here on pipes shorter than 1km of length. This is the case for the* `GasLib-4197` *dataset, which is based on a subset of the German gas transport. The operational constraints on the gas velocity are as follows: the minimum velocity shall be greater than 3 to 5 m s^{-1}, to minimize liquid fallout, but less than 20 to 25 m s^{-1} to minimize noise and prevent corrosion. Note that this may decrease to 15 m s^{-1} if the presence of corrosives in the gas is known. For a temperature of 15 ℃, and the specific gas constant of*

---

[1]GasLib is a collection of technical gas network descriptions as well as contract-based nomination data (gas flow and pressure specifications at entries and exits). This collection is based on real-world network data from the gas transport company Open Grid Europe GmbH. The data can be downloaded at `http://gaslib.zib.de`

$518.3 \, \mathrm{J\,kg^{-1}\,mol^{-1}}$, *we get that condition* (14) *is fulfilled for the minimum speed requirements for* 93.6% *of the* 2326 *pipes less than* 1*km. Note that in total, this represents* 61.5% *of all the pipes in that dataset. This indicates that the condition is met by a substantial sample of real-world pipes.*

For the analysis it is important to find accurate bounds for the source term. For $t \geq 0$ and the space variable x in order to describe the characteristic lines we define the $\mathbb{R}^2$-valued function $\xi_\pm(s, x, t)$ as the solution of the initial value problem

$$\begin{cases} \xi_\pm(t, x, t) = (t, x), \\ \partial_s \xi_\pm(t, x, t) = (1, \pm c). \end{cases}$$

This implies that

$$\xi_+(s, x, t) = (s, x + c(s - t)), \ \xi_-(s, x, t) = (s, x - c(s - t)).$$

Now we state our existence result.

Theorem 4.2. *Let $T > 0$ and $L > 0$ be given. Let numbers $\underline{p}$ and $\overline{p} > 0$ be given such that $0 < \underline{p} < \overline{p}$. Define the sets*

$$\Gamma_+ = \{0\} \times [0, L] \cup [0, T] \times \{0\},$$
$$\Gamma_- = \{0\} \times [0, L] \cup [0, T] \times \{L\}.$$

Define the points

$$P_0^\pm(t, x) = \Gamma_\pm \cap \{\xi_\pm(s, x, t), \ s \in \mathbb{R}\} \in \mathbb{R}^2.$$

For the t-component of $P_0^\pm(t, x)$ we use the notation $t_0^\pm(t, x) \geq 0$.

Let a continuous state R_+ on Γ_+, a continuous state R_- on Γ_- and a number $\lambda \in (0, 1)$ be given. Assume that there exists a number $\Delta t > 0$ such that the values of R_+ and R_- satisfy the inequalities

$$R_+(P_0^+(t, x)) - R_-(P_0^-(t, x)) \leq 2\overline{p}\left(1 - \frac{\theta\, c\,\Delta t}{2}\lambda^2\right), \tag{15}$$

$$R_+(P_0^+(t, x)) - R_-(P_0^-(t, x)) \geq 2\underline{p}\left(1 + \frac{\theta\, c\,\Delta t}{2}\lambda^2\frac{\overline{p}}{\underline{p}}\right). \tag{16}$$

Define the constant

$$\hat{U} = \frac{1}{2}\theta\, c\,\lambda^2 + \frac{g\, s_{lope}}{c}.$$

Assume that $s_{lope} \leq 0$ and

$$\hat{U} \geq 0, \tag{17}$$

$$\frac{(1 - \lambda)\, R_+(P_0^+(t, x)) + (1 + \lambda)\, R_-(P_0^-(t, x))}{2\,\Delta t\,\overline{p}} \leq -\frac{1}{2}\theta\, c\,\lambda^2 - \frac{g\,|s_{lope}|}{c} \tag{18}$$

and

$$(1 + \lambda)\, R_+(P_0^+(t, x)) + (1 - \lambda)\, R_-(P_0^-(t, x)) \geq 2\,\Delta t\,\overline{p}\,\hat{U} \tag{19}$$

for all $(t, x) \in [0, T] \times [0, L]$. Moreover, assume that Δt is sufficiently small in the sense that

$$\Delta t\left[\frac{\sqrt{5}}{2}\theta\, c\,\lambda + \frac{g\,|s_{lope}|}{c}\right] < 1. \tag{20}$$

Then with the given values of R_+ on Γ_+ and R_- on Γ_- that prescribe initial conditions at $t = 0$ and boundary conditions at $x = 0$ and $x = L$, the hyperbolic system (8) has a unique solution on $[0, \min\{T, \Delta t\}]$ that is given by continuous functions $R_+(t, x), R_-(t, x)$ for $t \in [0, \min\{T, \Delta t\}]$ and $x \in [0, L]$. The solution is subsonic and the absolute value of the Mach number is less than or equal to λ. The values of the pressure are contained in the interval $[\underline{p}, \overline{p}]$.

If $\Delta t \geq \frac{L}{c}$, thus in particular if (14) holds, the solution exists on the interval $[0, T]$.

Remark 4.3. *Note that our assumptions imply that the compatibility conditions for continuous functions are satisfied at $t = 0$ and $x = 0$, $x = L$ between the initial and the boundary data.*

Proof. Let a continuous function $R = (R_+, R_-)$ with $R_+, R_- \in C([0, T] \times [0, L], \mathbb{R})$ be given that satisfies the conditions (15), (16), (18), (19), as well as the box constraints (10)–(13). Define the operator $P := (P_+, P_-)$ with

$$P_\pm(R)(t, x) = R_\pm(P_0^\pm(t, x)) - \int_{t_0^\pm(t,x)}^t \left[\frac{1}{4}\theta\, c\, F(R_+, R_-) + \frac{g\, s_{lope}}{c} \frac{R_+ - R_-}{2}\right](\xi_\pm(s, t, x))ds.$$

Our first step is to check that $P(R)$ satisfies, in terms of physical variables, the box constraints for the pressure and the bound for the Mach number, that is

$$2\,\underline{p} \leq (P_+ - P_-)(R) \leq 2\,\overline{p}, \tag{21}$$

and

$$\left|\frac{(P_+ + P_-)(R)}{(P_+ - P_-)(R)}\right| \leq \lambda, \tag{22}$$

are satisfied. Note that since $\lambda < 1$ and $(P_+ - P_-)(R) > 0$, the relation (22) implies $P_+(R) > 0$ and $P_-(R) < 0$. Due to (17) we have

$$P_\pm(R)(t, x) \geq R_\pm(P_0^\pm(t, x)) - \left(t - t_0^\pm(t, x)\right)\left(\frac{1}{2}\theta\, c\, \lambda^2 + \frac{g\, s_{lope}}{c}\right)\overline{p}.$$

Moreover, we have

$$P_\pm(R)(t, x) \leq R_\pm(P_0^\pm(t, x)) + \left(t - t_0^\pm(t, x)\right)\left(\frac{1}{2}\theta\, c\, \lambda^2 + \frac{g\, |s_{lope}|}{c}\right)\overline{p}.$$

Hence if $t - t_0^\pm(t, x) \leq \Delta t$ and $s_{lope} \leq 0$, inequality (15) implies

$$(P_+ - P_-)(R) \leq R_+(P_0^+(t, x)) - R_-(P_0^-(t, x)) + \overline{p}\,\theta\, c\, \Delta t\, \lambda^2 \leq 2\,\overline{p}.$$

Similarly, we have the inequality

$$(P_+ - P_-)(R) \geq R_+(P_0^+(t, x)) - R_-(P_0^-(t, x)) - (t - t_0(t, x))\,\theta\, c\, \lambda^2\, \overline{p}.$$

Hence, (16) implies

$$(P_+ - P_-)(R) \geq 2\,\underline{p}.$$

and $P(R)$ satisfies (21). Furthermore, we have $(P_+ - P_-)(R) \geq 2\,\underline{p} > 0$. This implies that the Mach number constraint (22) can expressed as in (12)–(13), that is:

$$(1 - \lambda)\, P_+(R) + (1 + \lambda)\, P_-(R) \leq 0, \tag{23}$$
$$(1 + \lambda)\, P_+(R) + (1 - \lambda)\, P_-(R) \geq 0. \tag{24}$$

For the first inequality, we obtain

$$(1 - \lambda)\, P_+(R) + (1 + \lambda)\, P_-(R) \leq (1 - \lambda)\, R_+(P_0^+(t, x)) + (1 + \lambda)\, R_-(P_0^-(t, x))$$
$$+ 2\,\Delta t\left(\frac{1}{2}\theta\, c\, \lambda^2 + \frac{g\, |s_{lope}|}{c}\right)\overline{p}.$$

Due to (18), this implies

$$(1 - \lambda)\, P_+(R) + (1 + \lambda)\, P_-(R) \leq 0.$$

For the second inequality, we have

$$(1 + \lambda) P_+(R) + (1 - \lambda) P_-(R) \geq (1 + \lambda) R_+(P_0^+(t, x)) + (1 - \lambda) R_-(P_0^-(t, x))$$
$$- 2 \Delta t \left(\frac{1}{2} \theta c \lambda^2 + \frac{g \, s_{lope}}{c} \right) \overline{p}.$$

Due to (19), this implies

$$(1 + \lambda) P_+(R) + (1 - \lambda) P_-(R) \geq 0.$$

Remember that with $(P_+ - P_-)(R) > 0$, the inequality (22) implies that $P_+(R) > 0$, and $P_-(R) < 0$. By Lemma A.2 $P(R)$ is continuous.

So we can start a fixed-point iteration with the operator P where each iterate satisfies (21)–(22). It remains to show that the fixed-point iteration is convergent. However, this is standard. In fact for a continuous function that satisfies (21), (23)–(24), and $S_+ = R_+$ on Γ_+ and $S_- = R_-$ on Γ_- we have

$$|P_+(R) - P_+(S)|(t, x) \leq \frac{\theta c}{4} \int_{t_0^\pm(t, x))}^t |F(R_+, R_-) - F(S_+, S_-)| \, (\xi_+(s, t, x)) \, ds$$
$$+ \int_{t_0^\pm(t, x))}^t \left| \frac{g \, s_{lope}}{c} \frac{(R_+ - S_+) - (R_- - S_-)}{2} \right| (\xi_+(s, t, x)) \, ds.$$

Note that we can invoke Lemma A.1 to get the estimate

$$|P_+(R) - P_+(S)|(t, x) \leq \left[\frac{\sqrt{5}}{2} \theta c \lambda + \frac{g s_{\text{lope}}}{c} \right] |t - t_+^0(t, x)| \max\{|R_+ - S_+|, |R_- - S_-|\}.$$

For P_- a similar estimate holds. Hence, if $|t - t_0(t, x)| \leq \Delta t$, due to (20) we have

$$\Delta t \left[\frac{\sqrt{5}}{2} \theta c \lambda + \frac{g \, |s_{lope}|}{c} \right] < 1,$$

which implies that P is a contraction. Hence, Banach's fixed-point Theorem yields the existence of a continuous solution on the corresponding short time-interval contained in $[0, \Delta t]$.

Note that due to the construction, we have the upper bound $|t - t_0(t, x)| \leq \frac{L}{c}$. Hence, if the assumptions hold with $\Delta t \geq \frac{L}{c}$, we obtain a contraction on $[0, T] \times [0, L]$ which implies that the solution exists on the interval $[0, T]$ where T can be chosen arbitrarily large.

Thus, we have proved Theorem 4.2. □

Remark 4.4. *Analogously to Theorem 4.2, for boundary and initial data with L^∞-regularity we obtain L^∞-solutions that satisfy the PDE in the sense of the integral equation along the characteristic curves. These L^∞-solutions are particularly useful in the analysis of problems of optimal boundary control. For the proof, the fixed-point iteration has to be defined in the appropriate L^∞-spaces.*

5 Constrained exact controllability

In the operation of gas networks when the customer demand changes from an initially constant demand to a new constant demand, it is necessary to steer the system from a stationary initial state to a desired terminal state in such a way that the imposed state constraints for the pressure and velocity remain valid. While there are numerous results about exact controllability (see for example [9]), to our knowledge the exact boundary controllability with state constraints has not yet been analyzed for hyperbolic systems. Exact boundary controllability with control constraints has been studied for example in [8].

We want to analyze the problem of state–constrained exact boundary controllability between stationary states in the framework of continuous solutions on $\Omega = [0, T] \times [0, L]$. To this end, we divide this domain into four domains, as shown on Fig. 1. The stationary solutions of (5) are presented in Section 3. Note that an initial stationary state $R_{\pm}^{(0)}$ completely determines the system state on the triangle

$$D_{\mathrm{I}} := \{(t, x) : t \geq 0, \; x \in [0, L], \; c\,t \leq x, \; c\,t \leq L - x\}.$$

If the state constraints hold for the initial state, they are also satisfied on D_{I}. Similarly, for $T > L/c$, a desired stationary terminal state $R_{\pm}^{(T)}$ completely determines the system state on the triangle

$$D_{\mathrm{II}} := \{(t, x) : t \in [0, T], \; x \in [0, L], \; c\,(T - t) \leq x, \; c\,(T - t) \leq L - x\}.$$

Again if the state constraints hold for the terminal state, they are also satisfied on D_{II}.

In order to construct exact boundary controls that steer the system from $R_{\pm}^{(0)}$ to $R_{\pm}^{(T)}$, we define a new state $R_{\pm}^{\mathrm{mid}}$ on the I_{mid} segment which joins the inner vertices of the D_{I} and D_{II} triangles. More precisely, this segment is defined as:

$$I_{\mathrm{mid}} := \left[\frac{L}{2c}, T - \frac{L}{2c}\right] \times \left\{\frac{L}{2}\right\}.$$

One possibility for the values of $R_{\pm}^{\mathrm{mid}}$ is to use a convex combination of the values at the aforementioned vertices.

Now we introduce the boundaries for the following analysis: they are given by

$$\Gamma_{+}^{\mathrm{III}} := I_{\mathrm{mid}} \cup \left\{\left(T - \frac{y}{c}, y\right) \mid 0 \leq y \leq \frac{L}{2}\right\}, \quad \Gamma_{-}^{\mathrm{III}} := I_{\mathrm{mid}} \cup \left\{\left(\frac{y}{c}, y\right) \mid 0 \leq y \leq \frac{L}{2}\right\},$$

$$\Gamma_{+}^{\mathrm{IV}} := I_{\mathrm{mid}} \cup \left\{\left(\frac{y}{c}, L - y\right) \mid 0 \leq y \leq \frac{L}{2}\right\}, \quad \Gamma_{-}^{\mathrm{IV}} := I_{\mathrm{mid}} \cup \left\{\left(T - \frac{y}{c}, L - y\right) \mid 0 \leq y \leq \frac{L}{2}\right\}.$$

Now we can exchange the roles of t and x and consider a leftwards initial boundary value problem on the set

$$R^{\mathrm{III}} := [0, T] \times [0, \frac{L}{2}] \backslash (D_{\mathrm{I}} \cup D_{\mathrm{II}}),$$

with "initial" data from the stationary states $R_{\pm}^{(0)}$, $R_{\pm}^{(T)}$ on $\Gamma_{\pm}^{\mathrm{III}} \cap D_I$, $\Gamma_{\pm}^{\mathrm{III}} \cap D_{II}$ respectively and $R_{\pm}^{\mathrm{mid}}$ on I_{mid}. The PDE for the Riemannian invariants reads

$$(R_{\pm})_x \mp \frac{1}{c}(R_{\pm})_t = -\frac{1}{4}\theta F(R_+, R_-) - g\,s_{lope}\frac{R_+ - R_-}{2c^2}, \tag{25}$$

where F is defined in (7). The plus component of the boundary trace of these solutions at $x = 0$ yields a continuous boundary control $u_+(t)$ for $t \in (0, T)$. The existence of solutions for such a problem, with the solution satisfying the state constraints, is dealt with in Proposition 5.1, under appropriate smallness assumptions for $R^{(T)} - R^{(0)}$ and on θ and $|s_{lope}|$. The latter is addressed in (14), and the former is made precise in the forthcoming hypothesis (28)–(31).

Similarly, by considering a rightwards initial boundary value problem for the hyperbolic system

$$(R_{\pm})_x \pm \frac{1}{c}(R_{\pm})_t = -\frac{1}{4}\theta F(R_+, R_-) - g\,s_{lope}\frac{R_+ - R_-}{2c^2}, \tag{26}$$

on the set

$$R^{IV} := [0, T] \times [x_0, L] \backslash (D_{\mathrm{I}} \cup D_{\mathrm{II}}),$$

we obtain a continuous boundary control $u_-(t)$ for $t \in (0, T)$ as the minus-component of the boundary trace of these solutions at $x = L$.

(a) Boundaries for the R^{III} domain.
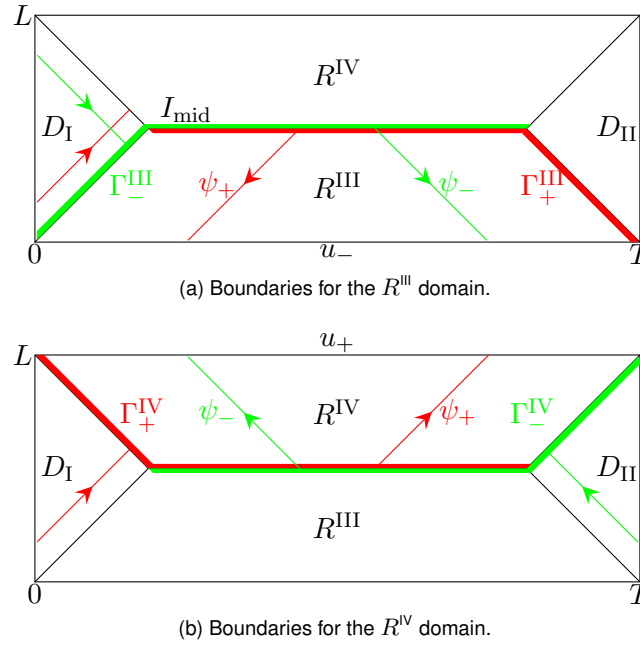

(b) Boundaries for the R^{IV} domain.

Figure 1: Domain and boundaries for the exact controllability boundary analysis.

Since we have reversed the roles of time and space, the integration is performed along the characteristics curves $\psi(y, t, x)$, which satisfy the following ODE:

$$
\begin{cases}
\psi_\pm(x, t, x) = (t, x), \\
\partial_y \psi_\pm(y, t, x) = (\pm c^{-1}, 1).
\end{cases}
\tag{27}
$$

These functions can be represented as

$$
\psi_\pm(y, t, x) = (t \pm c^{-1}(y - x), y).
$$

The following proposition contains sufficient conditions that guarantee the existence of continuous solutions of the corresponding Goursat-problems on R^{III} and R^{IV}, respectively.

Proposition 5.1. *Suppose that* $T > L/c$ *and* (14) *hold. Define*

$$
\tilde{U} = \frac{1}{2}\theta\lambda^2 + \frac{g}{c^2}|s_{\mathrm{lope}}|.
$$

Furthermore, we suppose that the steady continuous initial state $R_\pm^{(0)}$, *the steady terminal state* $R_\pm^{(T)}$, *and the values on* I_{mid} *are such that the following inequalities hold:*

$$
R_+(\mathbf{P}_+^0(t, x)) - R_-(\mathbf{P}_-^0(t, x)) \leq \bar{p}\left(2 - \tilde{U}L\right),
\tag{28}
$$

$$
R_+(\mathbf{P}_+^0(t, x)) - R_-(\mathbf{P}_-^0(t, x)) \geq \underline{p}\left(2 + \tilde{U}L\frac{\bar{p}}{\underline{p}}\right),
\tag{29}
$$

$$
(1 + \lambda)R_+(\mathbf{P}_+^0(t, x)) + (1 - \lambda)R_-(\mathbf{P}_-^0(t, x)) \geq L\,\bar{p}\tilde{U},
\tag{30}
$$

$$
(1 - \lambda)R_+(\mathbf{P}_+^0(t, x)) + (1 + \lambda)R_-(\mathbf{P}_-^0(t, x)) \leq -L\,\bar{p}\tilde{U},
\tag{31}
$$

where the initial boundary domain $\mathbf{P}_\pm^0(t, x)$ *is defined as*

$$
\mathbf{P}_\pm^0(t, x) = \begin{cases}
\left\{\Gamma_\pm^{\mathrm{III}} \cap \{\psi_\pm(y, t, x), y \in \mathbb{R}\}\right\} & \text{for the domain } R^{\mathrm{III}}, \\
\left\{\Gamma_\pm^{\mathrm{IV}} \cap \{\psi_\pm(y, t, x), y \in \mathbb{R}\}\right\} & \text{for the domain } R^{\mathrm{IV}}.
\end{cases}
$$

Then, there exists a unique continuous solution on the R^{III} *(resp.* R^{IV}*) domain for the hyperbolic system* (25) *(resp.* (26)*) with initial value on* $\Gamma_\pm^{\mathrm{III}}$ *(resp.* $\Gamma_\pm^{\mathrm{IV}}$*) that satisfies the box constraints* (9) *and* (11).

Proof. For $|M| \leq \lambda$ we have

$$\left| \frac{1}{2} \theta M |M| + \frac{g}{c^2} s_{\text{lope}} \right| \leq \tilde{U}.$$

Let us proceed with the analysis of the domain R^{III}, for which the initial conditions are $\Gamma_{\pm}^{\text{III}}$. The choice of ψ in (27) is such that

$$\frac{d}{dy} R_{\pm} \circ \psi_{\pm}(y, t, x) = \left((R_{\pm})_x \mp c^{-1} (R_{\pm})_t \right) \circ \psi_{\pm}(y, t, x)$$

$$= \left(-\frac{1}{2} \theta F(R_+, R_-) - g s_{lope} \frac{1}{c^2} \left(\frac{R_+ - R_-}{2} \right) \right) \circ \psi_{\pm}(y, t, x).$$

As in the proof of Theorem 4.2, we tackle the existence of solutions by using a fixed-point approach on $P :=$ (P_+, P_-), defined as follows:

$$P_{\pm}(R_{\pm}(t, x)) := R_{\pm}(P_{\pm}^0(t, x)) + \int_{x_{\pm}^0}^x \frac{d}{dy} R_{\pm} \circ \psi_{\pm}(y, t, x) dy,$$

with $P_{\pm}^0(t, x) := \Gamma_{\pm}^{\text{III}} \cap \{\psi_{\pm}(y, x, t), y \in \mathbb{R}\}$ is the initial boundary for the domain R^{III} (see Fig 1) and $x_{\pm}^0$ is the "space"-component of $P_{\pm}^0(t, x)$, where the argument (t, x) on $x_{\pm}^0$ is dropped since there is no ambiguity. Note that by construction of the domain R^{III}, we have

$$|x(t, x) - x_{\pm}^0(t, x)| \leq \frac{L}{2}. \tag{32}$$

Finally, it holds that $R_{\pm}(P_{\pm}^0(t, x)) = R_{\pm} \circ \psi(x_{\pm}^0, t, x)$.

Let a continuous function $R = (R_+, R_-)$ be given that satisfies the box constraints (10)–(13), and for which the hypothesis (28)–(31) and (14) hold. Let us denote the right-hand side in (25) by $f \circ R$. Then, rewriting this function in terms of the pressure p and Mach number M, we get

$$f(p, M) = -\frac{1}{2} \theta p M |M| - g s_{\text{lope}} \frac{p}{c^2},$$

which leads to the upper bound

$$|f| \leq \frac{1}{2} \theta \lambda^2 \bar{p} + g |s_{\text{lope}}| \frac{\bar{p}}{c^2} = \tilde{U} \bar{p}. \tag{33}$$

We continue our analysis by checking whether $P(R)$ satisfies the following constraints

$$2\underline{p} \leq (P_+ - P_-)(R) \leq 2\bar{p}, \tag{34}$$

and

$$\left| \frac{(P_+ + P_-)(R)}{(P_+ - P_-)(R)} \right| \leq \lambda, \tag{35}$$

on R^{III}. Note that if $(P_+ - P_-)(R) > 0$ and $\lambda < 1$, then the relation (35) implies $P_+(R) > 0$ and $P_-(R) < 0$. Starting with (34), we get:

$$P_+(R)(t, x) - P_-(R)(t, x) = R_+(P_+^0(t, x)) - R_-(P_-^0(t, x)) + \int_{x_+^0}^x f \circ R \circ \psi_+(y, t, x) dy$$

$$- \int_{x_-^0}^x f \circ R \circ \psi_-(y, t, x) dy.$$

Using (32) and (33), the magnitude of the difference of the integral terms can be bounded by $\tilde{U} L \bar{p}$. Then, invoking hypothesis (28) and (29), we get

$$2\underline{p} \leq P_+(R)(t, x) - P_-(R)(t, x) \leq 2\bar{p}.$$

Now let us move to the inequalities (35):

$$(1 + \lambda)P_+(R)(t,x) + (1 - \lambda)P_-(R)(t,x) = (1 + \lambda)R_+(P_+^0(t,x)) + (1 - \lambda)R_-(P_-^0(t,x))$$
$$+(1 + \lambda)\int_{x_+^0}^x f \circ R \circ \psi_+(y,t,x)\mathrm{d}y + (1 - \lambda)\int_{x_-^0}^x f \circ R \circ \psi_-(y,t,x)\mathrm{d}y.$$

Note that the sum of the integral terms is also bounded in magnitude by $\tilde{U} L \bar{p}$, for any value of $\lambda \in [-1, 1]$. Using hypothesis (30), we get

$$(1 + \lambda)P_+(R)(t,x) + (1 - \lambda)P_-(R)(t,x) \geq 0.$$

And similarly, using hypothesis (31), we have

$$(1 - \lambda)P_+(R)(t,x) + (1 + \lambda)P_-(R)(t,x) \leq 0.$$

Hence, along the characteristics, the constraints (34) and (35) are fulfilled as long as R satisfies the box constraints and the hypothesis (28)–(31) hold. Note that, by construction, $P_+(R)$ (resp. $P_-(R)$) is absolutely continuous on ψ_+ (resp. ψ_-).

We shall now show that P is a contraction. Remember that (34) and (35), with $\lambda < 1$, implies that $P_+(R) > 0$ and $P_-(R) < 0$. We now consider continuous functions $R_\pm$ and $S_\pm$ fulfilling (10) and (12)–(13), and such that $S_+ = R_+$ on Γ_+^{III} and $S_- = R_-$ on Γ_-^{III}. Following the usual approach for studying contraction properties, we have

$$|P_+(R) - P_+(S)|(t,x) \leq \frac{\theta}{4}\int_{x_+^0}^x |F(R_+, R_-) - F(S_+, S_-)| \circ \psi_+(y,t,x)\mathrm{d}y$$
$$+ \frac{gs_{\mathrm{lope}}}{2c^2}\int_{x_+^0}^x |R_+ - S_+ - R_- + S_-| \circ \psi_+(y,t,x)\mathrm{d}y.$$

Invoking Lemma A.1 yields the following estimate:

$$|P_+(R) - P_+(S)|(t,x) \leq \left[\theta\lambda\frac{\sqrt{5}}{2} + \frac{gs_{\mathrm{lope}}}{2c^2}\right]|x - x_+^0(t,x)|\max\{|R_+ - S_+|, |R_- - S_-|\}.$$

For P_-, the same estimate holds. Since $|x - x_+^0(t,x)| \leq \frac{L}{2}$ on $\mathrm{R}^{\mathrm{III}}$, using (14) we get

$$|P_\pm(R) - P_\pm(S)|(t,x) \leq \frac{1}{2}\max\{|R_+ - S_+|, |R_- - S_-|\}.$$

Hence Banach fixed-point theorem asserts the existence of a unique continuous solution, which satisfies the box constraints.

For the domain R^{IV}, the proof is along the same line. The hyperbolic system is (26), with initial conditions now on $\Gamma_\pm^{\mathrm{IV}}$. The operator $P := (P_+, P_-)$ on R^{IV} reads

$$P_\pm(R_\pm(t,x)) = R_\pm(P_\pm^0(t,x)) + \int_{x_\pm^0}^x f \circ \psi_\pm(y,t,x)\mathrm{d}y,$$

with $P_\pm^0(t,x) := \Gamma_\pm^{\mathrm{IV}} \cap \{\psi_\pm(y,x,t), y \in \mathbb{R}\}$. Note that the bound (33) is also valid for the term under the integral. Furthermore, the initial values $R_\pm(P_\pm^0(t,x))$ satisfy (28)–(31). Following the same steps as for R^{III}, we get that P_+ and P_- satisfy (34)–(35). Additionally, the contraction proof for P goes through whenever (14) holds. Hence, on R^{IV}, there is also existence and uniqueness of a continuous solution satisfying the box constraints. □

The above construction implies that with the continuous boundary controls u_+ at $x = 0$ and u_- at $x = L$, the initial boundary value problem with the initial state $R^{(0)}$ has a continuous solution R on $[0, T] \times [0, L]$ that satisfies the state constraint on $[0, T] \times [0, L]$ and the terminal constraint

$$R(T, x) = R^{(T)}(x).$$

Thus, we have shown the following theorem on local constrained exact controllability:

Theorem 5.2. *Assume that $T > L/c$, and that the characteristics of the pipe are such that the condition* (14) *is fulfilled. Assume that the steady initial state $R^{(0)}$, the steady terminal state $R^{(T)}$, and the* RIEMANN *invariants R^{mid} on I_{mid} are continuous, satisfy the state constraints and the inequalities* (28)–(31). *Then, the system can be steered by continuous boundary controls from the stationary state $R^{(0)}$ to the stationary state $R^{(T)}$ in the time T with a continuous state in such a way that the state constraints are satisfied on $\Omega = [0, T] \times [0, L]$.*

Proof. The proof has been sketched at the beginning of the section. The assumptions of Proposition 5.1 are satisfied. Hence Proposition 5.1 yields the existence of a solution on R^{III} and R^{IV}. The continuous boundary controls are then obtained from the boundary traces of the continuous state at $x = 0$ and $x = L$. □

6   Numerical experiments

We present some numerical results for the exact controllability between two stationary states, and investigate two cases: the first one is an increase in the mass flow and the second one is an inversion of the direction of the flow. The integral form of the systems (8) and (26) is considered. The numerical scheme consists of discretizing the right-hand side those systems of ODEs using the midpoint rule. To make this concrete, let us derive the expressions for the system (8). First we consider three points (t_i, x_i), (t_j, x_j), and (t_k, x_k), such that (t_k, x_k) is at the intersection of the ξ_+ and ξ_- characteristics starting from (t_i, x_i) and (t_j, x_j). Then, there exists Δ_+ such that $\xi_+(t_i + \Delta_+, x_i, t_i) = (t_k, x_k)$ and Δ_- such that $\xi_-(t_j + \Delta_-, x_j, t_j) = (t_k, x_k)$. Let $R_\pm^i := R_\pm(t_i, x_i)$, $R_\pm^j := R_\pm(t_j, x_j)$, and $R_\pm^k := R_\pm(t_k, x_k)$. The integral form of (8) over the interval $[t_i, t_i + \Delta_+]$ for R_+ is

$$\left[R_+ \circ \xi_+(s, x_i, t_i) \right]_{t_i}^{t_i + \Delta_+} = \int_{t_i}^{t_i + \Delta_+} \left[\frac{\theta\, c}{4}\, F(R_+, R_-) - g\, s_{lope}\, \frac{R_+ - R_-}{2c} \right] \circ \xi_+(s, x_i, t_i)\mathrm{d}s.$$

Using the midpoint rule for approximating the integral on the right-hand side yields

$$R_+^k - R_+^i = \frac{\Delta_+}{2} \left[\frac{\theta\, c}{4}\, (F(R_+^i, R_-^i) + F(R_+^k, R_-^k)) - g\, s_{lope}\, \frac{R_+^i - R_-^i + R_+^k - R_-^k}{2c} \right]. \qquad (36)$$

Similarly, we have the following relation for R_-^j and R_-^k:

$$R_-^k - R_-^j = \frac{\Delta_-}{2} \left[\frac{\theta\, c}{4}\, (F(R_+^j, R_-^j) + F(R_+^k, R_-^k)) - g\, s_{lope}\, \frac{R_+^j - R_-^j + R_+^k - R_-^k}{2c} \right]. \qquad (37)$$

Hence, the numerical scheme for computing the values of the RIEMANN invariants at (t_k, x_k) consists in finding a solution to the nonlinear (implicit) system formed by the previous two equations. Newton's method is then used to compute a solution to this system. For this, we first need to define a set of points $\{(t_k, x_k)\}$ at which those quantities are evaluated. Since the right-hand side involves both R_+ and R_-, the set of points must allow for the evaluation of both quantities. This is achieved by considering a "triangular" grid, constructed in the following way: for the D_I and D_II domains, N_D equidistant nodes are placed on the line segment corresponding to the initial (resp. terminal) state. Then, N_D equidistant line segments, parallel to the y-axis, slice the triangle D_I (resp. D_II) into $N_D - 1$ convex isosceles trapezoids. The nodes in the grid are defined as the intersection of

the characteristic lines starting from the N_D nodes located on the initial (resp. terminal) state and the afore-mentioned vertical line segments. This also implies that both RIEMANN invariants are defined at the nodes, as well as pressures and Mach numbers. The number of nodes on each line segment is decreasing by one when moving away from the initial (resp. terminal) state. The distance between two consecutive nodes on a given characteristic is $\Delta s = \frac{L}{2c(N_D-1)}$. Note that this quantity is an output for a given choice of grid, and not an input parameter for the construction of the grid.

The R_{III} and R_{IV} domains are also sliced into convex isosceles trapezoids by N_R horizontal line segments, between I_{mid} and the u_+ (resp. u_-) boundary. It is also the number of nodes on any horizontal line segment of length T_L, and hence gives the distance $\Delta t = \frac{L}{2c(N_R-1)}$ between nodes on I_{mid}. To simplify the numerical implementation, we round up the length of I_{mid} so that it is a multiple of Δt. Then, the number of nodes on I_{mid} is N_{mid} and the number of nodes on each boundary $u_\pm$ is $N_{\mathrm{mid}} + N_R$. The distance between two consecutive nodes on a given characteristic is $\Delta y = \frac{L}{2(N_R-1)}$.

One of the property enjoyed by our numerical solution is its reversibility along the characteristics. This is easy to see from the system (36)–(37): the right-hand side has the same expression for both R^i and R^j. Hence, changing the integration interval from t_k to $t_k - \Delta_+$ yields the same relation as (36), with just both sides negated. This implies that the boundary values computed by the forward/backward propagation of I_{mid} can be interpreted as control. Indeed, assuming that $N_R = N_D$, then integrating forward in time the pipe using those boundary values would give the desired terminal state. For example, this is not the case with the explicit or implicit Euler discretization. Another consequence is that values of R on $\Gamma_\pm^{\mathrm{III}}$ and $\Gamma_\pm^{\mathrm{IV}}$ must coincide, in particular outside of I_{mid}. By construction, this is true for either R_+ or R_-, and this was numerically verified for the other component of R at a very high numerical accuracy.

The setup for the numerical simulations is as follows: the pipe length $L = 1000$ km, $D = 1$ m, $T = 15$ °C, $R_s = 518.26$ J kg^{-1} K, $\lambda_{fric} = 2 \cdot 10^{-6}$. This gives $c = 386.44$ m s^{-1} and $T_L = 2587.71$ s. The large pipe length is there to further highlight the effect of the nonlinear source term.

Example 6.1. With this pipe, we first compute the controls for increasing the flow rate in the pipe from $q_0 = 100$ kg s^{-1} m^{-2} to $q_T = 1000$ kg s^{-1} m^{-2}, while keeping a pressure of $p = 50$ bar at $x = 0$. The associated
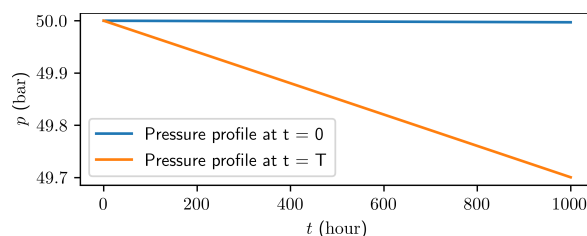

Figure 2: Pressure profiles in the pipe for the initial and terminal states, both being stationary.

stationary solutions yield the pressure drops displayed in Fig. 2. Since our analysis is in the regime of a rather low friction parameter and low mass flows, the nonlinearity of the pressure drop along the pipe is present, but hard to detect in Fig. 2.

We first study the evolution of the pressure and flow across time and space, as shown in Fig. 3. The triangular areas that appear flat are D_{I} on the right and D_{II} on the left. The main differences between the two different terminal times is the larger amplitude of the pressure, as well as a smoother transition of the mass flow from the initial value to the terminal one for $T = 10159s$ when compared to $T = 4540s$.

Now, we focus on the evolution of the RIEMANN invariants at the ends of the pipe as shown in Fig. 4. First, remember that due to the finite propagation speed, the values of the RIEMANN invariants are fixed (or pre-determined) by the initial and terminal states for some time. Namely, for R_+ this is the case at $x = 0$ for $t \in [T - T_L, T]$, and at $x = L$ for $t \in [0, T_L]$. For R_- this is the case at $x = 0$ for $t \in [0, T_L]$, and at $x = L$ for $t \in [T - T_L, T]$. There is a major difference in the control and behavior depends on whether $T - T_L < T_L$ holds. If this is the case, then on the time interval $[T - T_L, T_L]$ both RIEMANN invariants are determined by the
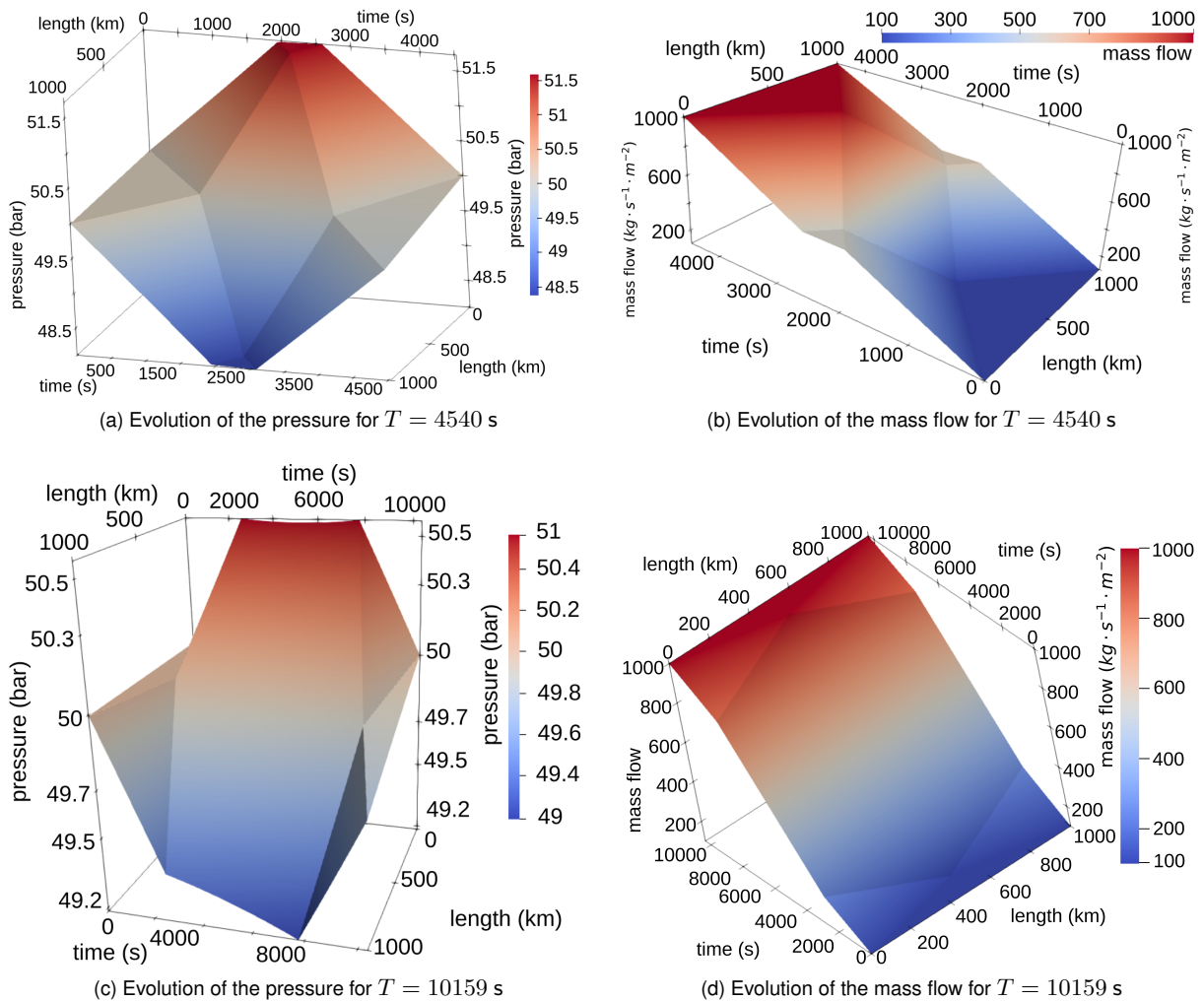
(a) Evolution of the pressure for $T = 4540$ s

(b) Evolution of the mass flow for $T = 4540$ s

(c) Evolution of the pressure for $T = 10159$ s

(d) Evolution of the mass flow for $T = 10159$ s

Figure 3: Evolution of the pressure and mass flow

initial and terminal states. Hence, there is no "choice" (in the sense of control input) of the RIEMANN invariants on that interval. This motivates the presentation of the numerical results with two terminal times: for the shorter time horizon $T = 4540$ s, $T - T_L < T_L$, whereas for the longer time horizon $T = 10159$ s this inequality does not hold. Two vertical lines, one for $t = T_L$ in blue, and one for $t = T - T_L$ in red, have been added to all the plots which depicts a time evolution.

In Fig. 4a and 4b, we see that R_+ at $x = 0$ transitions from its initial value to the one at the start of the pre-determined line segment in $[0, T - T_L]$, and at $x = L$ the same appears in $[T_L, T]$. For R_-, we find the same phenomenon, with the values of x reversed. In Fig. 4c and 4d, we observe that the evolution of the RIEMANN invariants occurs at a less steep slope thanks to the longer duration $T - T_L$ of the transitions. Also, in the time interval $[T_L, T - T_L]$, the values of both RIEMANN invariants can freely be selected, in contrast to the case $T = 4540$ s, where only one component of R can be selected at any time. While all plots depicted in Fig. 4 may appear to shown piecewise linear graphs only, this is just a visual effect due to the low friction and mass flow regime. Finally, note that the regularity of the RIEMANN invariants hinges on the choice of their values on the I_{mid} segment. Here we use a simple linear interpolation. We expect that a smoother transition would also smoothen the values of $R_\pm$ at the endpoints. However, such an investigation is beyond the scope of this paper.

In Fig. 5, the evolution of the pressure p and the Mach number M at the endpoints of the pipe are shown. The evolution of the pressure as shown in Fig. 5a and Fig. 5c can be divided into three phases: first a change from the initial values to a plateau-like phase, and then a transition to the terminal state values. The duration of the
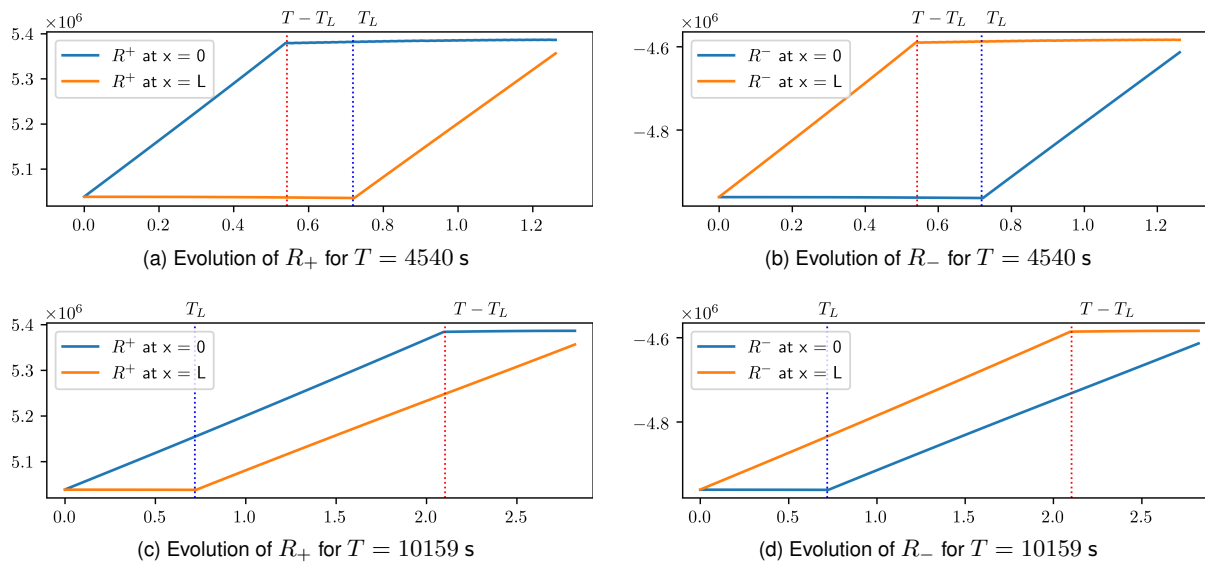
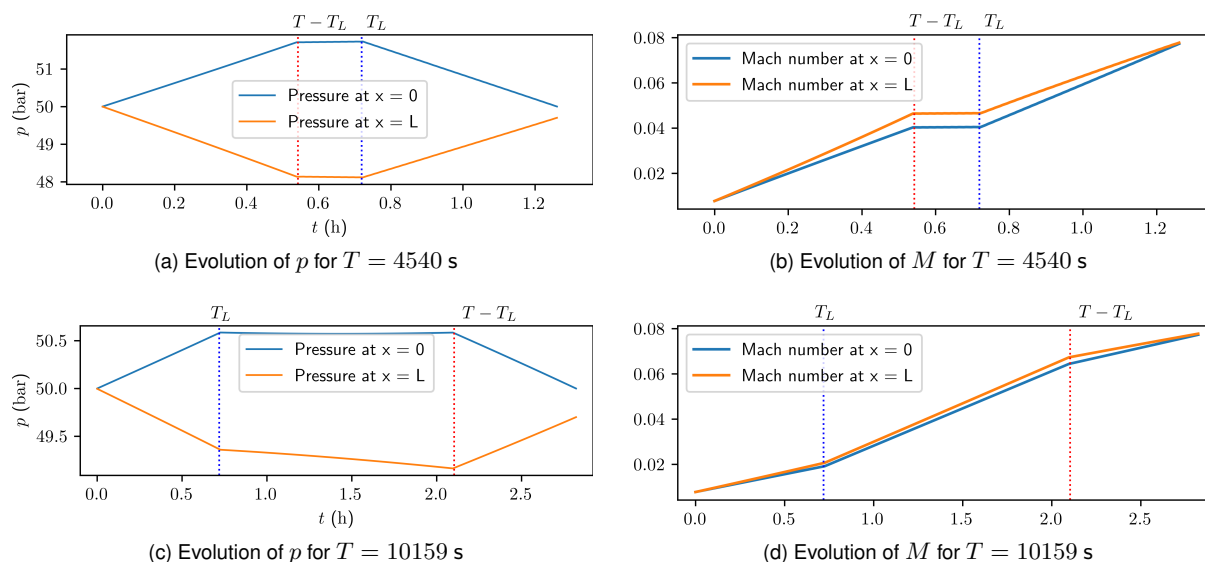Figure 4: Evolution of the RIEMANN invariants at the endpoints

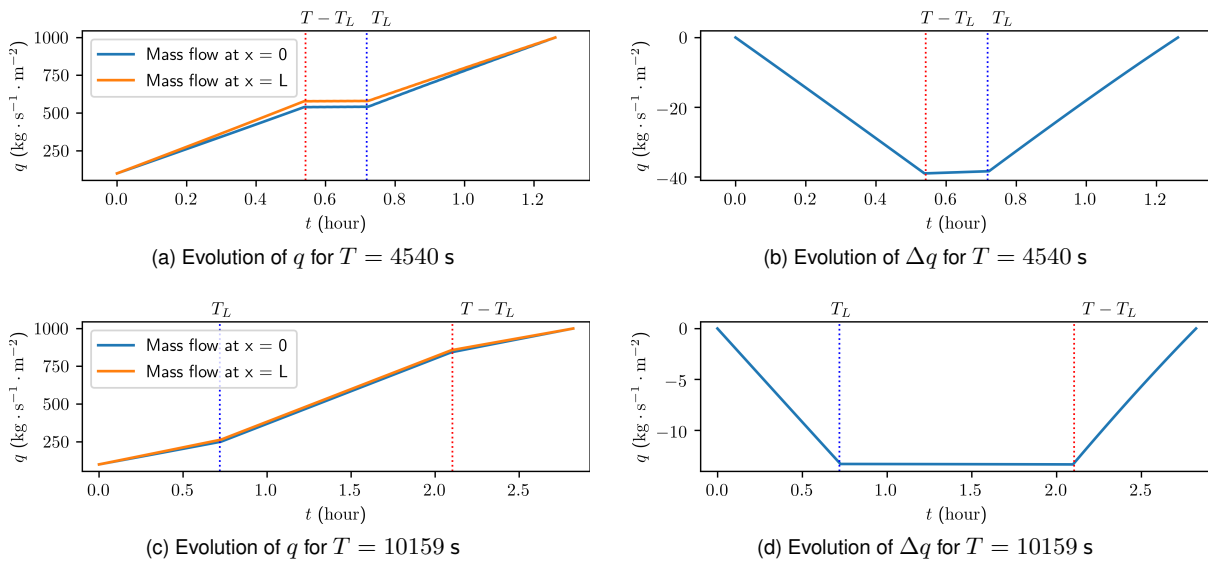Figure 5: Evolution of the pressure p and Mach number M at the endpoints

(a) Evolution of q for $T = 4540$ s

(b) Evolution of Δq for $T = 4540$ s

(c) Evolution of q for $T = 10159$ s

(d) Evolution of Δq for $T = 10159$ s

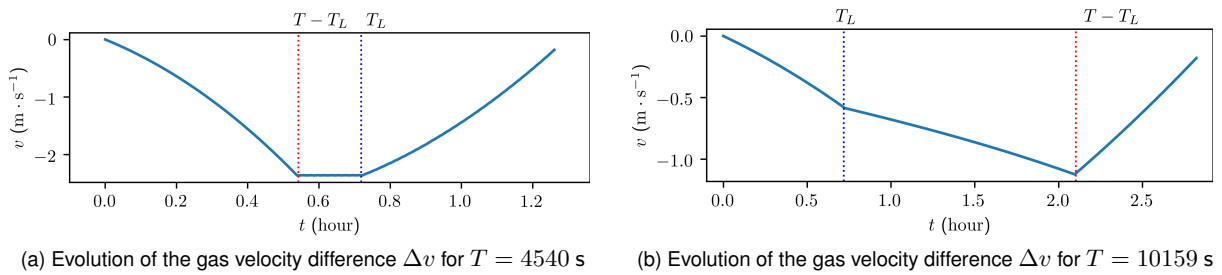Figure 6: Evolution of the mass flow q at the endpoints and the difference $\Delta q := q(\cdot, 0) - q(\cdot, L)$.

(a) Evolution of the gas velocity difference Δv for $T = 4540$ s

(b) Evolution of the gas velocity difference Δv for $T = 10159$ s

Figure 7: Difference in gas velocities $\Delta v := v(\cdot, 0) - v(\cdot, L)$ between the endpoints.

first and third phase is $\min\{T_L, T - T_L\}$ for each, and the second one lasts for the remaining time. Note that the variation in pressure is much smaller in Fig. 5c when compared to the one in Fig. 5a. For the Mach number M, the same behavior with 3 phases is present. Now, the difference between Fig. 5b and Fig. 5d is in the rate of change of the Mach number, with the extremal values being the same, respectively. In particular, remember that for $T = 4540$ s, the control input is predetermined on $[T - T_L, T_L]$. Hence, outside this time interval, the rate of change has to be larger in order to account not only for the reduction in terminal time, but also for this additional constraint.

In Fig. 6a and Fig. 6c, the evolution of the mass flow at the endpoints is depicted. The behaviour is quite similar to the one for the Mach number in Fig. 5b and Fig. 5d. The associated difference in input/output is highlighted in Fig. 6b and Fig. 6d. The evolution also follows again a three phases regime. Note that the difference Δq is about three times larger in magnitude for $T = 4540$ s than for $T = 10159$ s.

Finally, in Fig. 7a and Fig. 7b, the difference Δv in gas velocity at the end of the pipe is shown. The values depicted in Fig. 7a drop more rapidly and remain relatively constant in the time interval $[T - T_L, T_L]$, whereas in Fig. 7b, the change is comparable in all three time intervals.

Example 6.2. Let us now move on to the second scenario: a flow inversion in the pipe, from $q_0 = 1000 \, \mathrm{kg \, s^{-1} \, m^{-2}}$ to $q_T = -1000 \, \mathrm{kg \, s^{-1} \, m^{-2}}$, while keeping a pressure of $p = 50$ bar at $x = 0$. The associated pressure profiles are given in Fig. 8. The evolution of the pressure and mass flow rate are depicted in Fig. 9. Given a terminal time much larger than T_L, the flow reversal is rather smooth across the pipe, as one can see in Fig. 9b. In Fig. 9a, as expected, we observe that the pressure increases at $x = L$ and decreases at $x = 0$ to induce the switch.
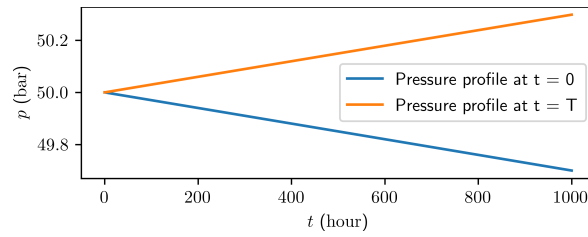
Figure 8: Pressure profile in the pipe associated with the initial and terminal state, both being stationary.

(a) Evolution of the pressure for $T = 10159$ s

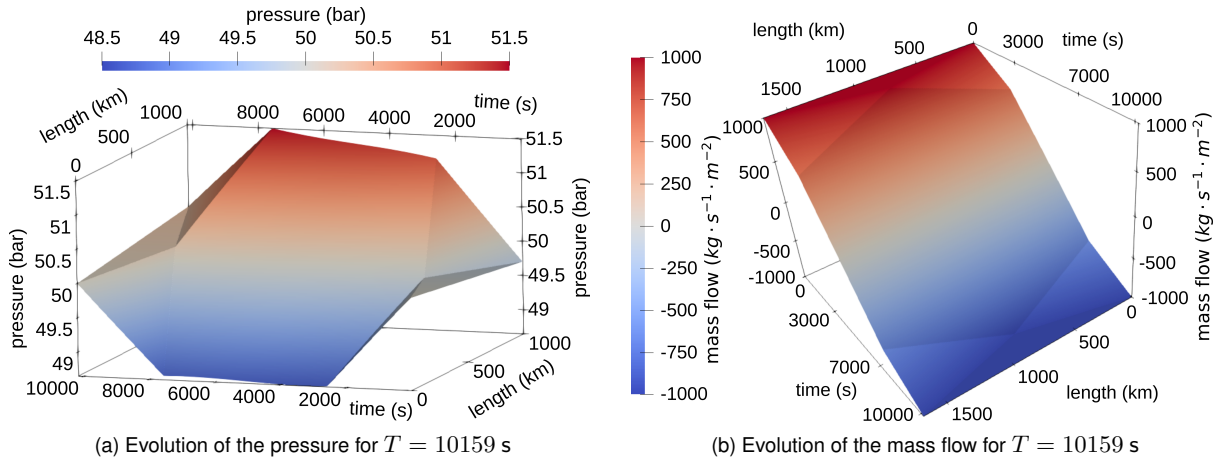(b) Evolution of the mass flow for $T = 10159$ s

Figure 9: Evolution of the pressure and mass flow.

As for the previous numerical analysis, we first focus on the evolution of the RIEMANN invariants in Fig. 10. The same three phase regime with $T - T_L > T_L$, is observed. The evolution of $R_\pm$ follows the same logic as before: outside of the pre-determined values, the RIEMANN invariants evolve according to the values on I_{mid} propagated through the R^{III} and R^{IV} domains.

This yields the pressure and Mach number as shown in Fig. 11. The main difference between the endpoints is the pressure, which evolves in a symmetric fashion between the endpoints of the pipe: a decrease (resp. increase) on $[0, T_L]$ followed by a plateau-like phase, and finally an increase (resp. decrease) on $[T - T_L]$ to the values given by the stationary solutions. Note how the pressure at $x = L$ transitions from a smaller value to a larger one at $x = 0$. The amplitude of the pressure remains small in this scenario. For the Mach number, in Fig. 11b, the difference between the endpoints remains small. The same can be stated about the evolution of the mass flow in Fig. 12, where the difference appears even smaller; see Fig. 12a. This is better appreciated on Fig. 12b, where the difference Δq is shown. Again we find an evolution with three phases, featuring a plateau-like phase in the middle which is only a few percents of the magnitude of the mass flow for the initial or terminal state.
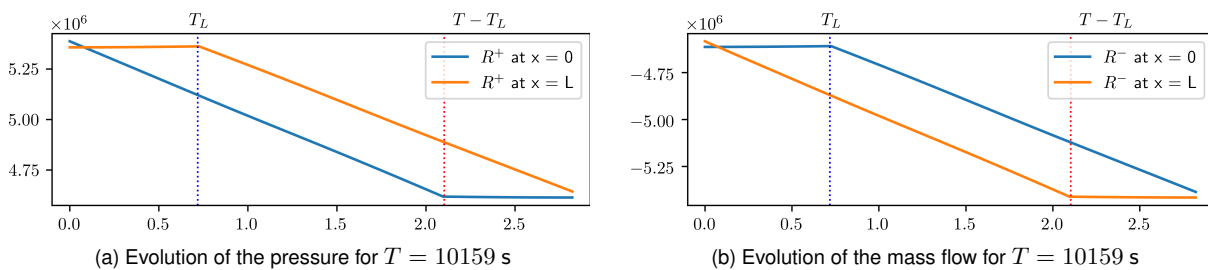

(a) Evolution of the pressure for $T = 10159$ s

(b) Evolution of the mass flow for $T = 10159$ s

Figure 10: Evolution of the RIEMANN invariants at the endpoints.

(a) Evolution of p for $T = 10159$ s

(b) Evolution of M for $T = 10159$ s
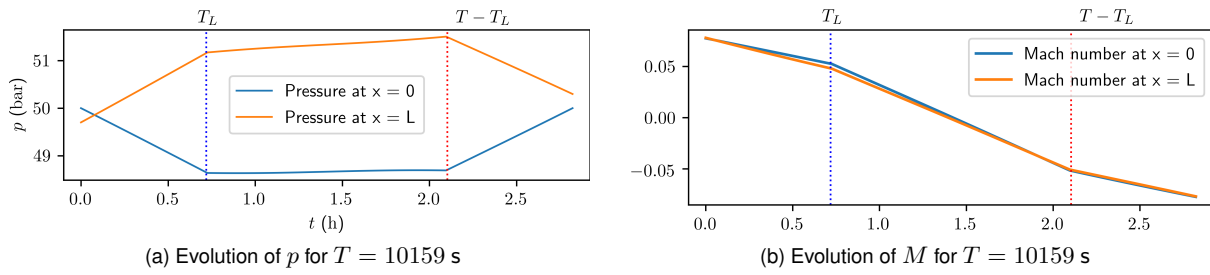
Figure 11: Evolution of the pressure p and Mach number M at the endpoints.

(a) Evolution of q for $T = 10159$ s

(b) Evolution of Δq for $T = 10159$ s

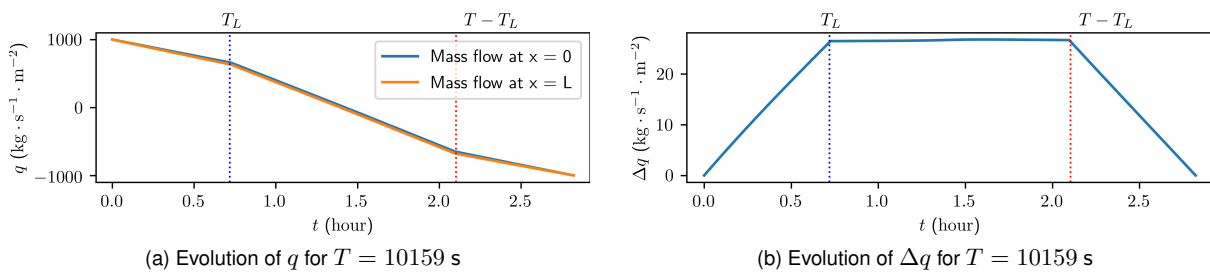Figure 12: Evolution of the mass flow q and the difference $\Delta q := q(\cdot, 0) - q(\cdot, L)$ at the endpoints.

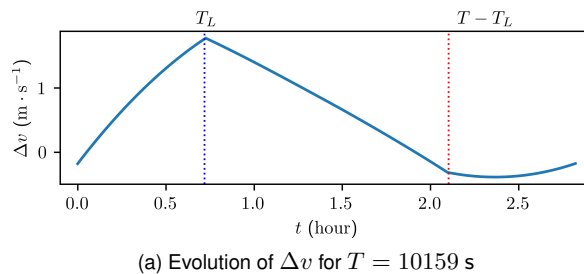(a) Evolution of Δv for $T = 10159$ s

Figure 13: Difference in gas velocities $\Delta v = v(\cdot, 0) - v(\cdot, L)$ between the endpoints

Finally, the difference Δv in gas velocity sheds some light on the difference between endpoints. Here the evolution is clearly nonlinear, and would be harder to to come by without observing the RIEMANN invariants first.

7 Conclusions

We have derived a semilinear model for gas pipeline flow from the quasilinear isothermal Euler equations. We have presented the corresponding stationary states not only for the case of horizontal pipes but also for the case of pipes with constant slopes. Moreover, also for the general case of pipes with constant slopes we have shown that for any given finite time horizon if the continuous initial data are sufficiently small, a continuous transient solution of the semilinear system exists that remains subsonic. In addition, the velocity of the gas remains below given a priori bounds and the pressure of the gas remains within a prescribed interval. This is important, since in the operation of gas pipelines, such bounds for the pressure and velocity occur regularly. We have shown that under certain smallness assumptions, the continuous solution exists even globally in time, that is for arbitrary large $T > 0$.

The constrained exact boundary controllability of the system was investigated. We have considered continuous solutions where the system is controlled from a given stationary state to a desired stationary state in such a way that the state constraints are satisfied everywhere throughout the process. In terms of the physical variables, the state constraints are box constraints for the pressure and an upper bound for the absolute value of the Mach number. These state constraints can be transformed to linear constraints in terms of the Riemann invariants.

We introduce a numerical scheme based on the midpoint rule to integrate the RIEMANN invariants on the characteristics. Finally, numerical simulations supporting the theoretical analysis have been shown. From those, we illustrate how the RIEMANN invariants on the boundaries evolve with respect to time. We highlighted the difference in behaviour whether the terminal time T is larger than $2L/c$ or smaller. In the latter case, the RIEMANN invariants invariants are determined on the time interval $[T - T_L, T_L]$ by the initial and boundary states. This result in a rather different behavior of the controls.

A   Technical lemmas

Lemma A.1. *Consider* $F(x,y) := (x+y)\left|\frac{x+y}{x-y}\right|$, *and* $\eta(x,y) := \frac{x+y}{x-y}$. *If* $x, u > 0$ *and* $y, v < 0$ *and* $|\eta(x,y)| \leq \lambda$ *as well as* $|\eta(u,v)| \leq \lambda$, *then it holds that* $|F(x,y) - F(u,v)| \leq \sqrt{20}\lambda \max\{|x-u|, |y-v|\}$.

Proof. Let $X := \{(w,z) \mid w > 0, z < 0\}$. Take $(x,y) \in X$ satisfying the hypothesis, and such that $x + y \neq 0$. Then, it holds that

$$\nabla F(x,y) = \frac{|x+y|}{(x-y)^2}\begin{pmatrix} x - y - 2y \\ x - y + 2x \end{pmatrix}. \tag{38}$$

Thus, the norm of the gradient can be estimated as follows

$$\|\nabla F(x,y)\| = \frac{|x+y|}{(x-y)^2}\sqrt{2(x-y)^2 + 4y^2 + 4x^2 + 4(x-y)^2}$$

$$= \frac{|x+y|}{x-y}\sqrt{6 + 4\frac{x^2+y^2}{(x-y)^2}}$$

$$\leq \frac{|x+y|}{x-y}\sqrt{10} = \sqrt{10}|\eta(x,y)|, \tag{39}$$

given that $1 > \frac{x^2+y^2}{(x-y)^2}$ on X. Now we consider $(x,y) \in X$ such that $x + y = 0$. In this case, by passing to the limit in (38), we infer $\nabla F(x,y) = 0$, hence the estimate (39) also holds on that line.
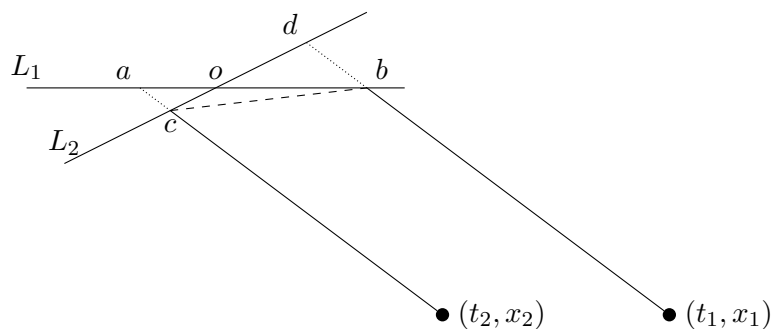
Figure 14: Projection near a corner

Note that we just shown that F is C^1, allowing us to invoke the mean value theorem, leading to the existence of $\tau \in [0, 1]$ such that

$$|F(x, y) - F(u, v)| = |\nabla F(\tau(x, y) + (1 - \tau)(u, v)) \cdot (x - u, y - v)|. \tag{40}$$

Note that the level sets of $|\eta|$ are convex on X. Since by hypothesis it holds that $|\eta(x, y)| \leq \lambda$ as well as $|\eta(u, v)| \leq \lambda$, we get

$$|\eta(\tau(x, y) + (1 - \tau)(u, v))| \leq \lambda.$$

Finally, using this relation in (39) gives us

$$\|\nabla F(\tau(x, y) + (1 - \tau)(u, v))\| \leq \lambda\sqrt{10}.$$

Inserting this into (40) yields

$$\begin{aligned} |F(x, y) - F(u, v)| &\leq \lambda\sqrt{10}\|(x - u, y - v)\| \\ &\leq \lambda\sqrt{20}\max\{|x - y|, |y - v|\}. \end{aligned}$$

$\square$

Lemma A.2. *Suppose that $P := (P_+, P_-)$ is one of the fixed-point operators defined on one of the domains $D_\mathrm{I}, D_\mathrm{II}, R^\mathrm{III}$, or R_IV. Suppose that the box constraints (21) and (22) on P are fulfilled. If the initial state $R(P_\pm^0)$ is continuous, then $P(R)$ is continuous on the corresponding domain $D_\mathrm{I}, D_\mathrm{II}, R^\mathrm{III}$, or R_IV, respectively.*

Proof. The operator P has a similar structure on all domains:

$$P_\pm(t, x) := R(P_\pm^0)(t, x) + G \circ R(t, x) - G \circ R(P_\pm^0(t, x)), \tag{41}$$

where G is the antiderivative of a continuous function. On each domain, the operator $P_\pm^0$ is an oblique projector on the initial boundary. That is, $P_\pm^0$ is an affine mapping. The term oblique projector indicates that the difference $(t, x) - P_\pm^0(t, x)$ does not lie in the orthogonal subspace to the range of $P_\pm^0(t, x)$, but is rather oblique to it. The difference $(t, x) - P_\pm^0(t, x)$ is on a direction d such that $\langle d, v \rangle \neq 0$, with v the direction of any piece of $P_\pm^0(t, x)$. Indeed, the characteristic lines are not orthogonal to neither the segment $\{\{0\}, [0, L]\}$ or $\{[0, T], \{0\}\}$. For instance the operator $P_\pm^0$ for the domain D_I is the matrix $\begin{pmatrix} 0 & 0 \\ -c & 1 \end{pmatrix}$. By construction of the operator P, the solution is absolutely continuous along the characteristics. Let us proceed by showing that each function in the right-hand side of (41) is continuous. This is clear for G by construction. For the remaining two terms, we show that $P_\pm^0$ is a Lipschitz operator. Note that if the initial boundary is made of one line segment (like for D_I and D_II), this property holds true. If the boundary consists of two line segments (like Γ^III), this requires a further step. In this case consider two points (t_1, x_1) and (t_2, x_2). Suppose that their image by the same projection operator is on different line segments, see Figure 14. Let b (resp. d) be the projection of (t_1, x_1)

onto L_1 (resp. L_2), and c (resp. a) be the projection of (t_2, x_2) onto L_2 (resp. L_1). Letting $\Pi_{\pm}^{L_i}$ be the oblique projector on L_i, we have

$$\|P_{\pm}^0(t_1, x_1) - P_{\pm}^0(t_2, x_2)\| = \|b - c\| \le \|b - o\| + \|o - c\| \le \|a - b\| + \|c - d\|$$
$$\le \|\Pi_{\pm}^{L_1}(t_1, x_1) - \Pi_{\pm}^{L_1}(t_2, x_2)\| + \|\Pi_{\pm}^{L_2}(t_1, x_1) - \Pi_{\pm}^{L_2}(t_2, x_2)\|.$$

Finally, since $R_{\pm}$ is continuous in space on the initial boundary, and G is continuous as well, this concludes the proof. □

References

[1] M. Banda, M. Herty, and A. Klar, *Gas flow in pipeline networks*, Networks & Heterogeneous Media 1, 41–56, 2006.

[2] M. Gugat, F.M. Hante, M. Hirsch-Dick, G. Leugering, *Stationary states in gas networks*, Networks and Heterogeneous Media 10, 295–320, 2015.

[3] M. Gugat, S. Ulbrich, *The isothermal Euler equations for ideal gas with source term: Product solutions, flow reversal and no blow up.*, Journal of Mathematical Analysis and Applications, 454, pp. 439–452, 2017.

[4] M. Gugat, G. Leugering, A. Martin, M. Schmidt, M. Sirvent, D. Wintergerst, *MIP-based instantaneous control of mixed-integer PDE-constrained gas transport problems*, Computational Optimization and Applications 70, 267–294, 2018.

[5] F. Hante, G. Leugering, A. Martin, L. Schewe, M. Schmidt, *Challenges in Optimal Control Problems for Gas and Fluid Flow in Networks of Pipes and Canals: From Modeling to Industrial Applications*, P. Manchanda, R. Lozi, A. H. Siddiqi, editors, Industrial Mathematics and Complex Systems: Emerging Mathematical Models, Methods and Algorithms, Springer Singapore, pp. 77–122, 2017.

[6] M. Herty, J. Mohring, V. Sachers, *A new model for gas flow in pipe networks*, Math. Meth. Appl. Sciences 33, 845–855, 2010.

[7] M. Hintermüller, N. Strogies, *Identification of the friction coefficient in a semilinear system for gas transport through a network*, Optimization Methods and Software, 35:3, 576–617, 2020

[8] J. Klamka, *Constrained exact controllability of semilinear systems*, Systems and Control Letters 47, 139–147, 2002.

[9] T.-T. Li, B.-Y. Zhang, *Global Exact Controllability of a Class of Quasilinear Hyperbolic Systems*, Journal of Mathematical Analysis and Applications 225, 1998, 289–311.

[10] M. Gugat, E. Zuazua, *Exact penalization of terminal constraints for optimal control problems* Optimal Control Applications & Methods, Vol. 37, No. 6 (2016), pp. 1329–1354

[11] M. Schmidt, D. Aßmann, R. Burlacu, J. Humpola, I. Joormann, N. Kanelakis, T. Koch, D. Oucherif, M. E. Pfetsch, L. Schewe, R. Schwarz, and M. Sirvent, GasLib – A Library of Gas Network Instances. Technical report, Nov. 2017.

[12] M. Schmidt, D. Aßmann, R. Burlacu, J. Humpola, I. Joormann, N. Kanelakis, T. Koch, D. Oucherif, M. E. Pfetsch, L. Schewe, R. Schwarz, and M. Sirvent, GasLib – A Library of Gas Network Instances. *Data*, 2(4): article 40, 2017.